Eur Biophys J (1999) 28: 380–392

ARTICLE

Valera P. Shcherbakov · M. Winklhofer

The osmotic magnetometer: a new model for magnetite-based magnetoreceptors in animals

Received: 18 May 1998 / Revised version: 11 February 1999 / Accepted: 11 February 1999

Abstract Homing pigeons and migratory birds are well known examples for animals that use the geomagnetic field for their orientation. Yet, neither the underlying receptor mechanism nor the magnetoreceptor itself is known. Recently, an innervated structure containing clusters of magnetite nanocrystals was identified in the upper beak skin of the homing pigeon. Here we show theoretically that such a cluster has a magnetic-field-dependent shape, even in fields as weak as the Earth's magnetic field; by converting magnetic stimuli into mechanical strain, the clusters can be assumed as primary units of magnetoperception in homing pigeons. Since the orientation of the strain ellipsoid indicates the direction of the external magnetic field, a cluster of magnetite nanocrystals also has the potential to serve as the basis of the so-called inclination compass of migratory birds. It is quantitatively demonstrated that the magnetic-field-induced shape change of a cluster can be amplified as well as counterbalanced by means of osmotic pressure regulation, which offers an elegant possibility to determine the magnetic field strength just by measuring changes in concentration.

Key words Superparamagnetism · Magnetic fluids · Ferrovesicle

Introduction

The old idea of a magnetic sensory system in animals that involves ferro(i)magnetic material was re-suggested by Lowenstam (1962), who discovered the iron-oxide magnetite (Fe_3O_4) in denticle capping of chitons, a group of recent mollusks. This idea has been further elaborated after the magnetic detection of permanent magnetic material in honeybees (Gould and Kirschvink 1978) and homing pigeons (Walcott et al. 1979) – animals for which a magnetic sense has been shown in numerous behavioral experiments [see Wiltschko and Wiltschko (1979) for a summary]. An additional argument for magnetite-based magnetoperception theories has been the electron microscopic identification of magnetite crystals (grain size $d \sim 30-50$ nm) in magnetic extracts of animal tissue, for example, of tuna (Walker et al. 1984, 1988) or salmon (Mann et al. 1988; Sakaki and Motomiya 1990). In rainbow trout (Walker et al. 1997), iron-rich particles (50 nm in size) were recently detected in cells that were considered candidates of magnetoreceptor cells as they were in close association with magnetically responsive nerves; however, it is not clear if the iron-rich particles in question are ferro(i)magnetic.

Not only magnetically stable single-domain (SD) grains have been found in this context: from low-temperature demagnetization experiments, Kirschvink and Gould (1981) inferred the occurrence of superparamagnetic (SP) magnetic material in worker honeybee abdomens. Electron microscopical investigations on magnetic extracts from worker bee abdomens indeed revealed superparamagnetic magnetite: one fraction with grain sizes between 15 nm and 30 nm, the other fraction with particles 3–5 nm in diameter (Kirschvink et al. 1993). SP magnetite within intact animal tissue was first found by Holtkamp-Rötzler et al. (1997), who investigated the upper beak of homing pigeons: The crystals, 2–5 nm in size, are arranged in densely packed clusters, typically 3 µm in size; the clusters seem to have a physiological meaning as they are connected to nerve fibers.

So far, however, magnetite-based receptors in animals are unknown. In all cases where magnetite was identified, its functional relation to magnetic field perception could not be clarified. The only case for a ferrimagnet-based magnetic sense of which the operating mechanism is known can be observed in magnetotactic bacteria (Blake-

Parts of this work have been presented at the 1998 AGU spring meeting in Boston and at the 1998 Gordon Conference on Bioelectrochemistry.

V.P. Shcherbakov
Geophysical Observatory "Borok", Borok Yaroslavskaja oblast, 151742, Russia

M. Winklhofer (✉)
Institut für Geophysik der Ludwig-Maximilians-Universität München, Theresienstrasse 41, D-80333 München, Germany
e-mail: michael@alice.geophysik.uni-muenchen.de

more 1975; Frankel and Blakemore 1980) and some eukaryotic algae (Torres de Araujo et al. 1986): intracellularly produced SD particles of magnetite or greigite (Fe_3S_4), so-called magnetosomes, are arranged in chains and thereby constitute minute compass needles which passively align the microorganism in the ambient field.

Several theoretical possibilities for animals to convert the magnetic field interaction of ferromagnetic material into a mechanical cell response have already been proposed (e.g. Yorke 1979; Presti and Pettigrew 1980; Kirschvink and Gould 1981; Semm and Beason 1990; Edmonds 1992; Kirschvink 1992a). Most of them are models of indirect transduction in that the direct reaction to the stimulus (magnetic field) is not an electric potential difference but is either a torque or a mechanical deformation of the unit containing the magnetic material; such magnetomechanical transformers in turn require mechanoreceptive units as actual transducers.

The simple torque mechanism due to alignment of organelle-sized bar magnets (SD particles) in the ambient field (Yorke 1979; Kirschvink and Gould 1981; Edmonds 1992; Kirschvink 1992b) may apply to animals that distinguish between magnetic north and south, as for example the sockeye salmon (Quinn and Brannon 1982). However, a torque transducer is not likely to be realized in migratory birds which were shown to employ a so-called "inclination compass" (Wiltschko and Wiltschko 1972), i.e., this compass seems to indicate the inclination angle of the field lines with respect to the gravitational force, but does not provide information about the polarity of the magnetic field. By means of an inclination compass, it is possible for the bird to distinguish between polewards and equatorwards; however, at the magnetic equator – where the field lines are horizontal – the polar direction is ambiguous. Wiltschko and Wiltschko (1972) showed that European robins, which are able to orient in inclined magnetic fields if other cues are absent, cannot orient in purely horizontal magnetic fields.

The superparamagnetic elastic rod transducer (Kirschvink and Gould 1981), in contrast, is a model for a purely axial transformer, independent of magnetic field polarity and compatible with the properties of the inclination compass. Kirschvink and Gould (1981) supposed that, under the influence of a magnetic field, SP particles embedded in an elastic matrix (e.g. attached to the cytoskeleton) will compress the matrix parallel to the applied field and stretch it along the two perpendicular axes. A characteristic of such a device is that the output signal is expressed in quite common biophysical cell variables like strain or additional pressure. These variables are, by definition, independent of polarity; moreover, strain or pressure receptors occur in almost every type of cell so that a transformation of the magnetic field response into a physiological signal would be straightforward. However, the mechanism related to the elastic rod transducer is energetically unfavourable as the body containing the SP material has to be magnetized perpendicular to its long axis [see Winklhofer (1998) for a critical analysis of the elastic rod transducer].

In the following we present a new model for a magnetoreceptor based on SP magnetite. The basic assumption in our model is that the SP particles found in the beak skin of homing pigeons in vivo are not embedded in an elastic matrix but dispersed in a liquid[1]. With this assumption, a cluster of SP particles may physically be described as a drop of a magnetic fluid (ferrofluid). In order to prevent such a drop from mixing with other cellular liquids, we assume it to be enclosed by a biological membrane (which is usually the case for cellular subsystems). Although in a completely different context, a similar system, called ferrovesicle, was technically synthesized by Bacri et al. (1996). In order to determine the bending elastic constant of lipid-bilayer membranes, they filled lipid-bilayer vesicles (i.e. closed membranes) with magnetic fluid and measured the magnetic-field-induced shape change of such vesicles.

As the basic mechanism underlying magnetoperception of homing pigeons, we consider the magnetic-field-induced shape change of an SP cluster. The deformation could then be transduced into an electric response by adjacent mechanosensitive receptors. Before the new model is quantitatively formulated, superparamagnetism as the underlying phenomenon is briefly described.

Superparamagnetism and magnetic fluids

Superparamagnetism (Elmore 1938; Néel 1949; Bean 1955) is the essential feature of the magnetoreceptor proposed here. An SP assemblage is characterised by relaxing into thermodynamic equilibrium in a short time (relaxation time $\tau \ll 1$ s) after a magnetic field change. If SP particles are embedded in a solid matrix, equilibrium is obtained by thermal fluctuation of the magnetic moments of individual particles; the relaxation time τ for this process, τ_N, can be expressed by the Néel-Arrhenius equation

$$\tau_N \sim f_0^{-1} \exp(E_b/k_B T) \quad (1)$$

where E_b is the energy barrier separating two local energy minimum states of a given particle, f_0 a frequency factor (for magnetite on the order of 10^9 s^{-1}), k_B Boltzmann's constant and T the absolute temperature. For magnetites as small as 10 nm, $E_b/k_B T \approx 1$ and therefore τ_N is on the order 10^{-9} s. In contrast to magnetic grains embedded in a rigid matrix, colloidal suspensions of ferromagnetic particles in a liquid can attain the state of thermal equilibrium also by Brownian motion. The corresponding relaxation time depends mainly on the viscosity η of the carrier liquid and the particle volume v

$$\tau_B \sim 3\eta v/k_B T \quad (2)$$

which for 10 nm-sized particles in water as carrier liquid ($\eta_0 \approx 0.01$ P) is on the order of 10^{-7} s. A magnetic fluid constitutes a stable phase if neighbouring magnetic parti-

[1] The other extreme case, i.e. the particles in an elastic medium, was treated by Winklhofer (1998)

cles are prevented from (permanent) agglomeration, since agglomeration causes separation of the solid phase from the carrier liquid. The solid phase then is no more liquid, the liquid no longer magnetic. To avoid agglomeration, the magnetic crystals in technically produced ferrofluids are coated by a so-called stabilizer; this substance adsorbed to the crystal surface increases the distance between two adjacent crystals and thereby reduces their mutual magnetostatic interaction energy, given by

$$W_{\mathrm{dip}} = (4\pi^2/9)\, M_{\mathrm{S}}^2\, (r/(1+\lambda/r))^3 \qquad (3)$$

(e.g. Berkovsky et al. 1993), where r denotes the radius of the magnetic crystal, λ the thickness of the coating layer and M_{S} the saturation magnetization, which for magnetite at room temperature is $M_{\mathrm{S}} = 480$ G; for maghemite (γ-Fe_2O_3), M_{S} assumes values between 370 and 390 G. Brownian motion will separate two agglomerating particles if W_{dip} does not exceed the order of $k_{\mathrm{B}}T$; from this condition the minimum thickness of the coating can be derived. For the small magnetite crystals detected in pigeon tissue ($r < 2.5$ nm), no coating layer is required to keep them dispersed in the carrier fluid.

One could also imagine that a ferrofluid is formed by "large" single-domain crystals of size $d_{\mathrm{SD}} \sim 50$ nm as they were extracted for example from salmon tissue. Indeed, the time scale for rotational diffusion, given by a modified Stokes law

$$\tau \sim 6\,\eta\,(M_{\mathrm{S}}\,H_0)^{-1} \qquad (4)$$

would be far below 1 s. However, from the stability condition for ferrofluids [Eq. (3)], the necessary coating thickness for steric repulsion is obtained as $\lambda_{\min} = 3\,d_{\mathrm{SD}}$, which makes the existence of a biogenic magnetic fluid consisting of "large" SD particles quite unlikely.

A magnetic fluid in an external magnetic field $\boldsymbol{H}_0$ is macrophysically characterized by its magnetization $\boldsymbol{M}$. The magnetization vector $\boldsymbol{M}$ is defined as $\Sigma_{i \in \mathrm{d}V}\, \boldsymbol{m}_i/\mathrm{d}V$, the spatial average over the magnetic moment vectors $\boldsymbol{m}$ in a volume element $\mathrm{d}V$. To a first-order approximation, the net magnetization $M = (\boldsymbol{M} \cdot \boldsymbol{H}_0)/H_0$ of a ferrofluid consisting of magnetically identical particles is given by

$$M(H_0) = \varphi\, M_{\mathrm{S}}\, L(x) \qquad (5)$$

(Elmore 1938), where φ denotes the packing density of magnetic material; $L(x)$ represents the Langevin function, $L(x) = \coth(x) - x^{-1}$, where $x = m\,H_0/k_{\mathrm{B}}T$ with $m = M_{\mathrm{S}}\,v$ being the magnetic moment of a single particle of volume v. x for the magnetite nanocrystals found in homing pigeons (grain size $\lesssim 5$ nm) amounts to less than 10^{-3} at room temperature in a 0.5 Oe magnetic field. $L(x)$ for $x \ll 1$ can be approximated by $x/3$, and the initial susceptibility, defined by $\chi_0 = (\partial M/\partial H_0)_{H_0 = 0}$, is given by $\chi_0 = \varphi\, v\, M_{\mathrm{S}}^2/3\,k_{\mathrm{B}}T$.

To determine the values of M or χ_0, φ has to be estimated. For this purpose, we assume that magnetic field receptors of animals are highly optimized, i.e. the organism produces a densely packed ferrofluid so as to maximize χ. From the transmission electron microscope pictures in Holtkamp-Rötzler et al. (1997) it can be seen that the particle density, in fact, is extremely high. If each particle is in direct contact with its nearest neighbours, the volume fraction φ of colloid particles equals 0.52 in the cubic-primitive packing ("cp") and 0.74 for the most dense packings, respectively. There is experimental evidence (Bacri et al. 1982) that colloid particles in dense ferrofluids are arranged in a cp-array, which is the configuration of lowest energy per dipole. The (microscopic) susceptibility of the biological ferrofluid then is obtained as $\chi_0^{\mathrm{cp}} = 0.06$. The effective susceptibility due to interactions, which for $\chi_0 \lesssim 0.2$ can be approximated by

$$\chi = \chi_0 + \frac{4\pi}{3}\,\chi_0^2 \qquad (6)$$

(see e.g. Blums et al. 1988), in this case amounts to $\chi = 0.08$, yielding a permeability of $\mu = 1 + 4\pi\chi = 2$.

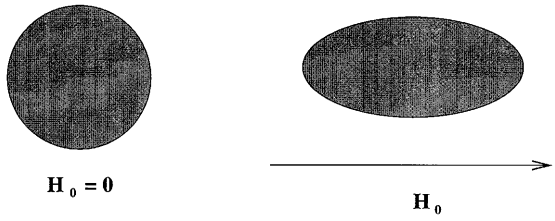

Fig. 1 Sketched deformation of a ferrovesicle according to the experiments by Bacri et al. (1996). In our model, a droplet of ferrofluid (*grey*) is enclosed by a biological membrane. In zero magnetic field the droplet has no net magnetization, and its initial shape is spherical (*left*). Under the influence of an external magnetic field $\boldsymbol{H}_0$, the ferrofluid is magnetized parallel to $\boldsymbol{H}_0$ and produces additional pressure in this direction, thereby deforming the sphere into an ellipsoid of revolution. The long axis of the ellipsoid indicates the axial direction of the external magnetic field but not its polarity; this model therefore is in accordance with the axial biological compass as deduced from behavioural experiments on migratory birds by Wiltschko and Wiltschko (1972)

Field-induced deformation of a ferrovesicle

Under the influence of a magnetic field, a ferrovesicle of spherical initial shape deforms to a prolate body with the long axis parallel to the magnetic field direction (Bacri et al. 1996) (Fig. 1). The reason for the mechanical deformation of a ferrofluid being magnetized is the additional pressure the ferrofluid produces in the direction of its magnetization to minimize the total energy by reducing the demagnetizing field. The response of the ferrovesicle to an external magnetic field is therefore completely different from that of the elastic rod transducer (Kirschvink and Gould 1981).

To estimate as to whether a ferrovesicle is suitable as a magnetic field receptor for animals, the physical theory of the ferrovesicle, first formulated by Bacri et al. (1996), has to be extended in a way that the effect of thermal fluctuations, which practically limit the receptor sensitivity, can be investigated. This requires an analytical expression for the total energy of a ferrovesicle.

Based on the experimental observation (Bacri et al. 1996) that an initially spherical ferrovesicle of radius R_0 in a weak external magnetic field H_0 deforms into a slightly elongated prolate ellipsoid of revolution ($a > b = c$, $k = b/a$, $\varepsilon = \sqrt{1-k^2}$), its eccentricity corresponding to mechanical and thermal equilibrium, ε_{eq} and $\bar{\varepsilon}$, respectively, can be determined by accounting for the following energy terms:

1. Magnetostatic energy

$$W_m = -\frac{1}{2}(\chi_{||}\cos\theta^2 + \chi_\perp \sin\theta^2) H_0^2 V \tag{7}$$

where V is the volume of the ferrovesicle, θ the angle of $\boldsymbol{H}_0$ with respect to the long vesicle axis, and $\chi_{||}$, $\chi_\perp$ are the apparent susceptibilities parallel and perpendicular to the applied field, which are related to χ, the intrinsic susceptibility of the ferrofluid, via $1/\chi_{||} = 1/\chi + N_{||}$ and $1/\chi_\perp = 1/\chi + N_\perp$; for a prolate spheroid, the demagnetizing factor parallel to the long axis is

$$N_{||} = 2\pi k^2 \varepsilon^{-3}(\log(1+\varepsilon) - \log(1-\varepsilon) - 2\varepsilon) \tag{8}$$

(e.g. Landau and Lifshitz 1984); $N_\perp$, the demagnetizing factor perpendicular to the long axis, is related to $N_{||}$ by $N_{||} + 2N_\perp = 4\pi$. The jump in magnetic normal traction across the surface of a magnetized body is obtained as $p_m = 2\pi M_n^2$, $M_n = \boldsymbol{M}\cdot\boldsymbol{n}$, where $\boldsymbol{n}$ is the outward unit vector normal to the surface and $\boldsymbol{M}$ the magnetization of the ferrofluid (Rosensweig 1985); at the poles of a uniformly magnetized sphere

$$M_n = \frac{3}{4\pi}\frac{\mu-1}{\mu+2} H_0 \tag{9}$$

2. Bending energy

$$W_b = \pi K_c (14/3 - 4a\,c_0 + (4/3 + a^2 c_0^2) k^2 + (2 + a^2 c_0^2 k^2)\,\mathrm{arcsin}(\varepsilon)/\varepsilon k - 4a\,c_0 k^2\,\mathrm{atanh}(\varepsilon)/\varepsilon) \tag{10}$$

(see Appendix A), where K_c is the bending rigidity of the vesicle membrane [for lipid bilayers, $K_c \sim 10\,k_B T$ (Sackmann 1994)] and c_0 its spontaneous curvature, which allows for possible structural differences between the inner and outer side of a membrane; for a symmetrical membrane (i.e. both sides are identical), $c_0 = 0$. A spontaneous curvature can be generated, e.g. by the adsorption of proteins or by changing the surface charge density (Sackmann 1994). Equation (A1) in Appendix A shows that the bending energy can be decreased by increasing c_0.

3. Energy required to change the vesicle volume

$$W_v = \Delta p (V - V_0) = (4\pi/3)(a^3 k^2 - R_0^3)\Delta p \tag{11}$$

where Δp is the thermodynamic pressure difference between the outer and the inner medium, $\Delta p = p(\rho, T)_{ext} - p(\rho, T)_{int}$, and V_0 the volume in the absence of an external field. Since Δp is due to concentration differences across the cell membrane, we set $\Delta p = \Delta\pi$, where $\Delta\pi$ is the osmotic pressure difference.

4. Stretching elastic energy

$$W_s = \kappa_s (\Delta A)^2 / A_0 \tag{12}$$

where $\Delta A = A - A_0$ is the change in surface area and κ_s is the elastic area stretching modulus. For egg lecithin bilayers, κ_s was measured as 140 dyn/cm (Kwok and Evans 1981). For weak deformations one can assume the lateral tension in the membrane, $\gamma = \kappa_s \Delta A/A_0$, as nearly constant, and the stretching elastic energy for the prolate ellipsoid of revolution then simplifies to

$$W_s' = \gamma_0 A_0 = 2\pi a^2 k (k + \varepsilon^{-1}\arcsin\varepsilon)\gamma_0 \tag{13}$$

Typical values of γ_0 are on the order of 10^{-4} dyn/cm (Evans and Rawicz 1990).

Mechanical equilibrium shape

In the following, two shape changes of the sphere are considered, where we assume that the energy contributions due to shearing can be neglected:

1. The volume is constant during deformation. This is the case when the membrane is completely impermeable. Since the sphere is a minimum surface, work needs to be done to enlarge its surface area. Minimizing the total energy with respect to ε leads to the equilibrium eccentricity for small deformations ($\varepsilon \ll 1$) and weak magnetic fields (i.e. $H^2 R_0/\gamma \ll (280\pi(\mu+2)^3)/((\mu-1)^2(16+29\mu))$):

$$\varepsilon_{eq}^2\big|_{\Delta V=0} \simeq \frac{2\pi M_n^2}{2(6 - c_0 R_0) K_c / R_0^3 + 2\gamma_0 / R_0} \tag{14}$$

The numerator in Eq. (14) represents the magnetic pressure jump across the droplet surface according to Eq. (9), the denominator is the sum of elastic stresses in the membrane, which counteract magnetic pressure. Expression (14) is equivalent to the deformation law derived by Bacri et al. (1996), which was based on the balance of normal forces along the vesicle membrane.

2. The surface area is constant during deformation. As the vesicle becomes more elongated, its volume can decrease without a change in surface area ($\Delta V/V \simeq -\varepsilon^4/15$); shrinking is accompanied by the diffusion of water through the membrane. This is the more realistic scenario than that depicted under 1, for the following reasons. First, the membrane can be regarded as unstretchable compared to its high flexibility with respect to bending. Second, even if devoid of specific channels for water, cellular membranes are highly permeable to water owing to the smallness of the water molecule. In addition to that, there is a tension limit causing lysis [3–4 dyn/cm according to Kwok and Evans (1981)], which is equivalent to a relative increase in area of 2–3%. Thus, for the deformation of a sphere into a prolate ellipsoid under the constraint $\Delta V = 0$, a

value for $\Delta A/A_0$ of 3% corresponds to an axial ratio a/b of about 1.5, which suggests that large deformations under this constraint rather destroy the vesicle.

In the following, we consider deformations with constrained surface area. For small eccentricities and weak magnetic fields we arrive at

$$\varepsilon_{\mathrm{eq}}^2\big|_{\Delta A=0} \simeq \frac{2\pi M_n^2}{2(6-c_0 R_0) K_\mathrm{c}/R_0^3 - \Delta\pi} \tag{15}$$

In comparison with Eq. (14), the membrane tension $2\gamma_0/R_0$ is now replaced by the (negative) osmotic pressure difference $\Delta\pi$, in accordance with the Laplace formula for spheres.

Thermal equilibrium shape

Each of the values of $\varepsilon_{\mathrm{eq}}$ obtained from Eq. (15) represents a minimum of the total energy of a vesicle described by a specific set of parameters $\nu=(H, \mu, K_\mathrm{c}, R_0, c_0, \Delta\pi)$. Owing to thermal fluctuations, however, values of ε related to higher vesicle energies are possible, too. Therefore, the thermodynamic equilibrium value of ε has to be determined. According to the ergodic theorem, the time average of ε^n (here of interest: $n=1, 2$) for a given set ν can be obtained by averaging over all possible configurations (ε, θ) for this vesicle with the Boltzmann distribution as probability density:

$$\langle\varepsilon^n\rangle = Z_{\varepsilon,\theta}^{-1} \int_0^1 \varepsilon^n Z_\theta(\varepsilon) \exp(-\beta W_{\mathrm{el}}(\varepsilon))\,\mathrm{d}\varepsilon \tag{16}$$

with $\beta=k_\mathrm{B}T$, the partition sum over θ

$$Z_\theta(\varepsilon) = \int_0^\pi \exp(-\beta W_\mathrm{m}(\varepsilon,\theta)) \sin\theta\,\mathrm{d}\theta \tag{17}$$

and $Z_{\varepsilon,\theta}$, the partition sum over both ε and θ, defined by

$$Z_{\varepsilon,\theta} = \int_0^1 Z_\theta(\varepsilon) \exp(-\beta W_{\mathrm{el}}(\varepsilon))\,\mathrm{d}\varepsilon \tag{18}$$

W_{el} represents the two sums $W_\mathrm{b}+W_\mathrm{v}$ (constraint: $S=\mathrm{const}$) and $W_\mathrm{b}+W_\mathrm{s}$ (constraint: $V=\mathrm{const}$), respectively. The thermally induced variance of the vesicle shape is given by $\sigma_\varepsilon^2=\langle\varepsilon^2\rangle-\langle\varepsilon\rangle^2$. After having thus determined the thermal equilibrium value of vesicle eccentricity, $\langle\varepsilon\rangle:=\bar{\varepsilon}$, the thermally induced deviations of the long vesicle axis from the axis of $\boldsymbol{H}_0$ can be obtained from

$$\langle\cos^2\theta\rangle = Z_\theta^{-1} \int_{-1}^1 \cos^2\theta \exp(-\beta W_\mathrm{m}(\bar{\varepsilon},\theta))\,\mathrm{d}\cos\theta \tag{19}$$

With Eq. (7) rewritten dimensionless as $-(\Delta m\cos^2\theta + m_\perp)$ where $\Delta m=\beta(\chi_\parallel-\chi_\perp)H_0^2 V/2 \geq 0$, the integration of Eq. (19) leads to

$$\langle\cos^2\theta\rangle = \left(\frac{2\sqrt{\Delta m/\pi}\exp(\Delta m)}{\mathrm{Erfc}\imath(\sqrt{\Delta m})} - 1\right)\Big/(2\Delta m) \tag{20}$$

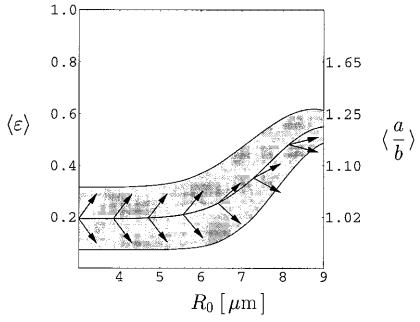

Fig. 2 Thermal equilibrium value and fluctuations of ferrovesicle eccentricity as a function of vesicle radius R_0. The *inner solid line* represents $\langle\varepsilon\rangle$ according to Eq. (16) (the right *y*-axis shows the corresponding axial ratio $\langle a/b\rangle$ on a nonlinear scale). The *grey area* above/below this line indicates the $\pm1\sigma_\varepsilon$ range, defined by $W_{\mathrm{tot}}(\bar{\varepsilon}\pm\sigma_\varepsilon)-W_{\mathrm{tot}}(\bar{\varepsilon})=1\,k_\mathrm{B}T$. A *pair of arrows* symbolizes the thermally induced deviations of the long vesicle axis from the external field direction, i.e. $W_\mathrm{m}(\bar{\varepsilon},\pm\sigma_\theta)-W_\mathrm{m}(\bar{\varepsilon},0)=1\,k_\mathrm{B}T$; the angle between the two arrows amounts to $2\arccos(\sigma_{\cos\theta})$. One can see that the long vesicle axis is randomly oriented for weakly elongated vesicles ($\sigma^2_{\cos\theta}\approx1/3$ for $R_0<6$ µm), whereas is more and more aligned with the field direction for increasing vesicle sizes. Parameter values: $H_0=0.5$ Oe, $\mu=2$, $K_\mathrm{c}=10\,k_\mathrm{B}T$, $c_0=0$, $\Delta\pi=0$

where $\mathrm{Erfc}\imath(x)$ is the imaginary error function. Because of $\langle\cos\theta\rangle=0$, one gets $\sigma^2_{\cos\theta}=\langle\cos^2\theta\rangle$. If the long vesicle axis is completely aligned with $\boldsymbol{H}_0$ then $\sigma^2_{\cos\theta}=1$, while random orientation in three dimensions is characterized by $\sigma^2_{\cos\theta}=1/3$.

Figure 2 shows the thermal equilibrium shape for a ferrovesicle as a function of the vesicle radius. The magnetic fluid is assumed to have a permeability of 2. Since magnetic energy is proportional to volume whereas bending energy depends on the surface area, the magnetic field does not come into effect until a vesicle has a certain size. In the example presented by Fig. 2, we see that vesicles with radii below 6 µm undergo frequent fluctuations in shape and orientation, while those with radii above 6 µm are noticeably influenced by the external field: vesicle elongations increase and at the same time the long axis is more and more aligned with the external field.

Figure 3a demonstrates that a large enough ferrovesicle can be used to measure magnetic field intensity. The thermal equilibrium value of its axial ratio shows a distinct increase with field strength H_0 even for intensities as low as the geomagnetic field. However, fluctuations of the axial direction are relatively large. In the next paragraphs, it is shown how the strain of a single ferrovesicle can be enlarged and thereby fluctuations in the axial direction can be reduced.

Role of osmotic pressure

According to Eq. (15), an increase in the osmotic pressure outside the ferrovesicle yields higher vesicle elongations. In Figure 3b and c this is shown for the ferrovesicle from Figure 3a. Now it can be seen that not only the magnetic-

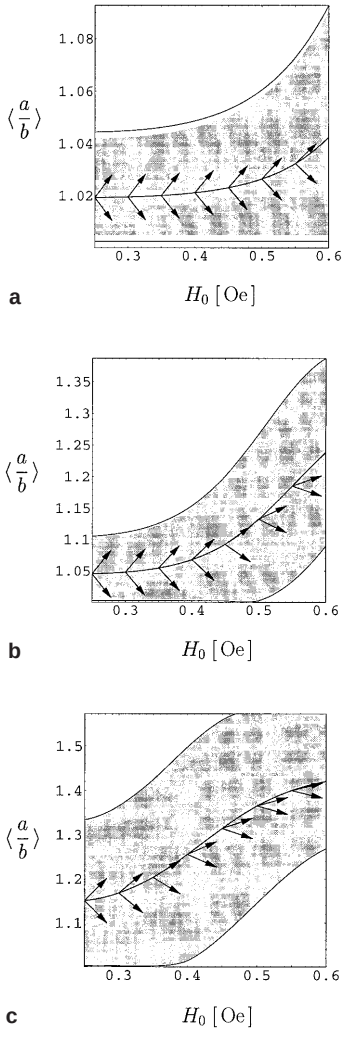

Fig. 3 a–c Field dependence of the vesicle shape. A ferrovesicle's axial ratio $\langle a/b\rangle \pm 1\,\sigma_{a/b}$ is plotted as a function of the external field H_0 for different values of $\Delta\pi$, the osmotic pressure difference (outside minus inside). **a** $\Delta\pi = 0$; **b** $\Delta\pi = 0.02$ dyn/cm^2; **c** $\Delta\pi = 0.025$ dyn/cm^2. Parameter values: $\mu = 2$, $K_c = 10\,k_BT$, $R_0 = 6$ µm, $c_0 = 0$

field-dependent strain is enlarged, but also the axial direction better defined.

From Eq. (15) another method to measure changes in magnetic field intensity can be deduced: counterbalance a magnetic-field-induced shape change by a corresponding change in osmotic pressure such that the shape before the field change is restored. This working principle, a constant-strain mode, has the advantage that possible geometric constraints can be overcome, for example, if there is no room for a vesicle to become elongated in a certain direction.

A further possibility to determine magnetic field strength by means of osmotic pressure regulation ensures from a phenomenon called vesicle instability. To depict this possibility, we first consider a normal vesicle containing a non-magnetic solution. The spherical vesicle shape is stable if the osmotic pressure inside is larger than outside, and the pressure difference $\Delta\pi$ is balanced by a tensile membrane stress γ. As long as the external pressure exceeds the inner pressure by not more than a certain threshold value $\Delta\pi^{\mathrm{crit}}$, the sphere is still an equilibrium shape. It will deform into an elongated body, however, when the external excess pressure $\Delta\pi$ exceeds

$$\Delta\pi^{\mathrm{crit}} = (2K_c/R_0^3)\,(6 - c_0 R_0) \qquad (21)$$

(Helfrich 1973) (for non-negative values of c_0)[2].

For vesicles filled with a magnetic fluid, the transition from weakly to the highly elongated also depends on magnetic field strength H_0 and therefore can be used as a measure of H_0. Further, the long axis of a ferrovesicle subject to shape instability coincides statistically with the axis of the external magnetic field, which is a necessary demand we make on our model to explain the birds' inclination compass.

Let the threshold pressure be defined as the osmotic pressure difference $\Delta\pi^*$ at which $\mathrm{d}\varepsilon_{\mathrm{eq}}/\mathrm{d}\Delta\pi$ assumes a maximum value. Then the field dependence of the threshold can be approximated by

$$\Delta\pi^* \approx \Delta\pi^{\mathrm{crit}} - 6(2\pi)^{3/2}\left(\frac{3(\mu-1)}{4\pi(\mu+2)}\right)^3 \sqrt{\Delta\pi^{\mathrm{crit}}}\,H_0 \qquad (22)$$

From Eq. (22) one can see further that a small vesicle yields higher absolute values for the threshold shift, whereas for a large vesicle the relative shift is larger, e.g., the relative change $(\Delta\pi^*(H_0+\delta H) - \Delta\pi^*(H_0))/\Delta\pi^*(H_0)$ for a vesicle of size $R_0 = 3$ µm amounts to 1% at $H_0 = 0.5$ Oe and $\delta H = 0.05$ Oe but to about 4% for a vesicle of double diameter. Supposing that $\Delta\pi$ can be adjusted to a high precision, it is possible to use osmotic pressure regulation also as a means to detect the intensity of the magnetic field.

Figure 4 shows the axial ratio of a vesicle as a function of the osmotic pressure difference across the ferrovesicle membrane. At $\Delta\pi < \Delta\pi^*$, a vesicle of radius 3 µm is obviously too small to exhibit a distinguishable orientation in the geomagnetic field (see also Fig. 2). By increasing $\Delta\pi$ above $\Delta\pi^*$, the vesicle is subject to shape instability and deforms into a highly elongated body, the long axis of which is now far better aligned with the magnetic field; in this example, $\Delta\pi^*$ is shifted by an amount of 0.017 dyn/cm^2 below $\Delta\pi^{\mathrm{crit}}$.

It is clear that active participation by the organism is required to control the process of field axis determination. There are several advantages of such a device. First, the reception unit does not need to be active all the time, but can be activated when required; also the precision in measuring the field axis can be specifically enlarged by controlling $\Delta\pi$ – this can be regarded in correspondence with the well-known experience of focusing one's sensory perception on a specific object. Second, an external quan-

[2] From Eq. (21), the so-called condition for vesicle instability, one can also see that it is possible to force a prolate shape at constant $\Delta\pi$ just by increasing the value of c_0 above $c_0^{\mathrm{crit}} = 6/R_0$. The prolate shape for $c_0 > c_0^{\mathrm{crit}}$ is favoured since the curvature can assume its large value of spontaneous curvature over most of the bilayer area (Helfrich 1973)

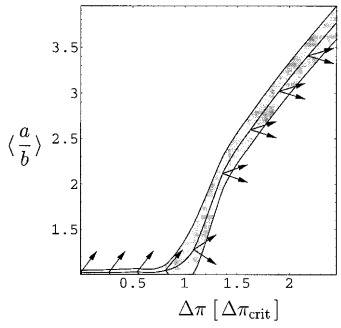

Fig. 4 The way the axial osmotic magnetometer works in the "shape-instability mode". A ferrovesicle's axial ratio $\langle a/b \rangle \pm 1\,\sigma_{a/b}$ is plotted as a function of the osmotic pressure difference $\Delta\pi$ across the vesicle membrane in units of $\Delta\pi^{\rm crit} = 12\,K_{\rm c}/R_0^3$ [see Eq. (21)]. Here, the vesicle radius R_0 is only 3 µm, which (judging from Fig. 2 with $\Delta\pi = 0$) is too small to yield a distinct alignment in magnetic field direction. However, a much better defined orientation can be achieved by increasing the osmotic pressure difference above $\Delta\pi^{\rm crit}$, where shape instability sets in. Parameter values: $H_0 = 0.5$ Oe, $\mu = 3$, $K_{\rm c} = 10\,k_{\rm B}T$, $R_0 = 3$ µm, $c_0 = 0$; $\Delta\pi^{\rm crit} = 0.184$ dyn/cm^2

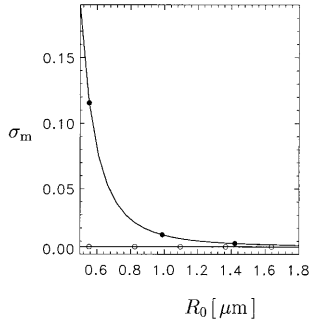

Fig. 5 Magnetic pressure $\alpha_{\rm m} = 2\pi M_n^2$ [dyn/cm^2] produced by initially spherical ferrovesicles of varying radii R_0 in an external magnetic field $H_0 = 0.5$ Oe. *Open circles*: vesicle containing a homogeneous ferrofluid of permeability $\mu = 2$ [M_n calculated according to Eq. (9)]; *filled circles*: vesicle containing a ferrofluid ($\mu = 2$) with a large SD particle of size $d = 100$ nm in its centre [M_n calculated according to Eq. (24)]

tity can be measured in quite a simple way just by regulating an internal parameter which the cell can handle easily. Here, the internal control parameters are the osmotic pressure difference and the corresponding concentration difference Δn, which, according to van't Hoff's law, are related by

$$\Delta\pi = \Delta n\,RT \tag{23}$$

with $R = k_{\rm B}\,L_{\rm A}$, where $L_{\rm A}$ is Avogadro's number. For the example shown in Fig. 4, a change in molar concentration of about 10 nM is related to 0.2 dyn/cm^2. Since this concentration change is relatively small, the proposed reception unit can work quite fast.

Amplification of M_n^2 by an SD core

Numerous behavioural studies on homing pigeons and honeybees indicate that these animals might be influenced by fluctuations of magnetic field intensity on the order of one part in 10^3 or even less (see Wiltschko and Wiltschko 1995). Provided that the intensity fluctuations indeed were the cause for the observed behaviour, sophisticated neuronal signal processing methods could be an explanation of such a highly sensitive magnetic field detection, for other senses like seeing or hearing owe their remarkable capabilities especially to complex neuronal processing steps in the central nervous system. Of course, this also raises the question of how the sensitivity of the single receptor cell can be enhanced. Here we propose a slight structural modification of the ferrovesicle which is not more than a single magnetically stable SD particle in the centre of a ferrovesicle. The idea is:

1. This particle, which can be considered as a compass needle, will be aligned with the external magnetic field $\boldsymbol{H}_0$.
2. The dipole field of that particle is superimposed on $\boldsymbol{H}_0$, thereby amplifying the the magnetic pressure exerted on the vesicle membrane, which can be used to increase the sensitivity of the ferrovesicle to magnetic field changes.

The first statement is easy to justify. According to Eq. (4), the Brownian diffusion time of an SD particle is less than 10^{-3} s in a medium of viscosity not too different from that of water, while since the Néel relaxation time of SP grains of 10 nm in diameter is on the order of 10^{-8} s, the SD grain can be considered as a permanent magnet situated in the ferrofluid. Such a modified ferrovesicle can be regarded as an extension of the torque detector model as suggested by Yorke (1979) or Kirschvink and Gould (1981), which is based on mechanical rotation of SD particles in a viscous environment. However, replacing the non-magnetic viscous medium by a ferrofluid essentially changes the properties of the whole configuration. Owing to the phenomenon of magnetic levitation (see, e.g. Rosensweig 1985), the SD particle would be repelled from the inner vesicle boundary, and we will show that, in case the size of the SD particle is not less than one tenth of the vesicle size, it is bound to the central part of the ferrofluid droplet.

The details of the calculations to support statement 2 are given in Appendix B; the result is presented in Fig. 5, showing the magnetic pressure produced by the ferrofluid with an "SD core" (solid circles) compared to the case of a homogeneous ferrofluid (open circles). One can see that the SD core does amplify the magnetic fluid pressure in the direction of the external field. At the interface between ferrofluid and vesicle membrane, the magnetization normal component of a spherical ferrovesicle with an SD particle in its centre is given by

$$M_n = \chi\,\frac{24\pi\,M_{\rm S} + 3H_0\,(2 + q^3 + 2\,\mu(q^3 - 1))}{q^3\,(2\,\mu + 1)\,(\mu + 2) - 2\,(\mu - 1)^2} \tag{24}$$

(see Appendix B), where q is the ratio of the vesicle radius to the radius of the SD particle. There is a size limit for this kind of receptor, which depends on the threshold grain size $d^{\mathrm{SD-PSD}}$, above which the single-domain state is no longer stable and collapses into a magnetic vortex configuration. For roughly equivalent particles of magnetite, $d^{\mathrm{SD-PSD}} \lesssim 100$ nm (Fabian et al. 1996), which limits the favourable size of an SD-cored ferrovesicle to about 1–2 µm.

One cannot a priori assume that the SD particle occupies the central region of the ferrofluid droplet; there are two forces able to drive it out of the centre: gravitation and thermofluctuations. For small vesicles ($R_0 < 10$ µm), the gravitational energy can be neglected because of its little effect compared to that of Brownian motion; this can be seen from the inequality $R_0\, q_{\mathrm{m}}\, g\, v \ll kT$, where q_{m} is the density of magnetite (~ 5 g/cm^3), g is the gravitational acceleration and v is volume of the SD particle. On the other hand, when Brownian motion drives the SD particle from its central position in the ferrofluid droplet towards the surface, the SD particle will be repelled from the surface. This remarkable phenomenon, called magnetic levitation, is due to the interaction of the permanent magnetic poles with the induced poles on the boundaries of a ferrofluid. Usually, magnetic levitation is observed for a macrobody immersed in a fluid (see e.g. Rosensweig 1985). For minute vesicles (about 1 µm in size), however, even an SD particle (the size of which is only one order of magnitude less than that of the vesicle) can be subject to repulsion forces and thus has a tendency to occupy the central region. This can be demonstrated by making use the approximation described, for example, by Bastovoj et al. (1988): we replace the actual magnetic field H by H_0, the magnetic field due to a magnet in vacuum, and have the ferrofluid magnetization as $M = \chi H_0$. According to Bastovoj et al. (1988), the expression for the repulsion force then simplifies to

$$\boldsymbol{F} = -(8\pi)^{-1} \oint_S (\mu - 1)\, H_0^2\, \boldsymbol{n}\, \mathrm{d}S \qquad (25)$$

where S denotes the surface of the particle. This formula was numerially evaluated for a small spherical SD particle immersed in a spherical ferrofluid droplet to obtain repulsion force as a function of h, the displacement of the particle from the centre; the corresponding potential $U(h)$ is shown in Fig. 6 (the details of the calculations are given in Appendix C). According to the Boltzmann distribution, the probability of finding a grain at a distance h from the centre is proportional to $\exp(-U(h)/kT)$ and, consequently, the particle is bound to the central region of the droplet.

Having in mind that in some magnetic extracts of animal tissues relatively large SD particles (50 nm in size) were found (e.g. Walker et al. 1984; Sakaki and Motomiya 1990) and provided that each such grain previously had been the central part of a ferrovesicle, it is possible that SP grains were not observed, either because of their smallness or as a result of the magnetic extraction techniques applied in these studies, which could have been designed especially for the extraction of highly permanent particles but not for (super-)paramagnetic material.

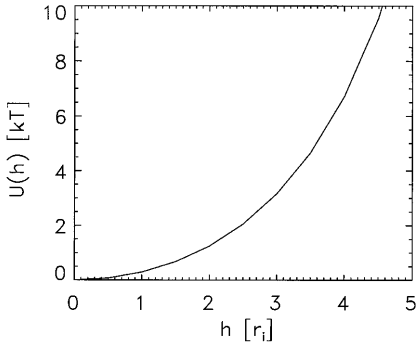

Fig. 6 Potential energy of an SD particle ($r_{\mathrm{i}} = 50$ nm) within a ferrofluid droplet ($\mu = 3$, $R_0 = 0.5$ µm) as a function of its radial displacement h/r_{i} from the centre of the droplet

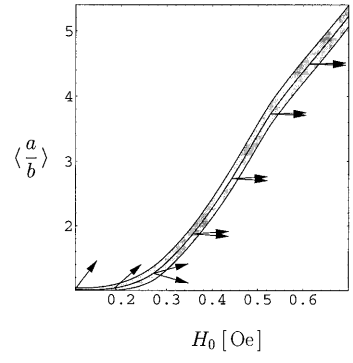

Fig. 7 Magnetic field dependence of the axial ratio $\langle a/b \rangle \pm 1\sigma_{a/b}$ of a vesicle containing a high-density ($\mu = 25$) ferrofluid. Over the relevant intensity range of the geomagnetic field, the ferrovesicle agglomerate reacts with marked shape changes. However, in comparison with the ferrofluid droplets investigated by Bacri and Salin (1982), which respond to a field threshold by a pronounced shape instability (e.g., a/b jumps from a value ≈ 1 to a value greater than 5), the transition here proceeds comparatively inconspicuously. The reason for the non-appearance of shape instability here is the presence of a membrane, since the bending energy acts in strong opposition to magnetic pressure and thus smoothes such strong effects. Parameter values: $R_0 = 5$ µm, $K_{\mathrm{c}} = 10\, k_{\mathrm{B}} T$, $c_0 = \Delta\pi = 0$

High-density magnetic fluids

A remarkable possibility to measure a certain field value using magnetic fluids arises from the investigations by Bacri and Salin (1982). They determined the threshold field strength H^{crit} above which the shape of a ferrofluid droplet of high magnetic permeability ($\mu \gtrsim 14$) jumps from slightly to highly elongated. The special thing about this observed instability is that values of H^{crit} are on the order of only 1 Oe, which makes this mechanism interesting for animals. Let us suppose that the organism has N individual field sensors at its disposal, each of which jumps at a different threshold H_j^{crit} and let the individual H_j^{crit} be distributed roughly evenly over the relevant field range $\bar{H} = 0.3$–0.6 Oe; the resulting sensitivity to detect a certain Earth magnetic field strength may then be written $H_0/\delta H \sim N/0.3$. This means a considerable enhancement

of sensitivity compared to processing methods based on signal stacking, which yield an increase in signal-to-noise ratio only proportional to $\sqrt{N}$.

Although it is not clear if animals can produce ferrofluids of high permeability, it is interesting to consider the theoretical deformation law for a ferrovesicle filled with a high-permeability ferrofluid.

Figure 7 shows the response of a vesicle containing a high-permeability ferrofluid ($\mu = 25$, $R_0 = 3.5\ \mu m$) to a magnetic field change. Although this ferrovesicle becomes highly elongated, the deformation curve does not exhibit a distinct jump as would be the case without an enclosing membrane; instead, the transition from weakly to highly elongated is smeared over a field range. Yet, a high-density fluid would provide a very compact device to measure the geomagnetic field.

Possible set of droplets to measure field direction

Electrophysiological responses stimulated by changes in the external magnetic field have been recorded from specific cells connected to the optic nerve system of pigeons (Semm et al. 1984; Semm and Demaine 1986). Those studies demonstrated a striking selectivity of individual cells for their response to different stimuli, i.e. the cells are specified in a sense that each one shows a distinct peak in its response if the inclination of the applied field lies in a particular range, which varies between the cells. Such a feature can easily be explained by means of elongated ferrofluid droplets. We assume that there is a set of N droplets engineered to measure the inclination in a way that sensitive fibres around the droplets create planes whose inclinations, in the coordinate frame linked with Earth's gravitation, gradually changes to cover the interval $(0, \pi)$. Let these fibres excite when the elongated part of the droplet gets in touch with them. As far as the long axes of the ellipsoid always follows the external field direction, it would send the required information, for example to the visual system. Therefore, a set of $2N$ receptor cells can provide the required two-dimensional base for compass orientation.

Summary and conclusions

1. The work was stimulated by the detection of an innervated structure containing clusters of magnetite nanocrystals in the beak skin of the homing pigeon (Holtkamp-Rötzler et al. 1997). Here we demonstrate by theoretical modelling that the clusters can serve as the basis of magnetic field perception, since the cluster shape is magnetic field dependent, even in a magnetic field as weak as the Earth's magnetic field.
2. To describe a cluster theoretically, we use the ferrovesicle (Bacri et al. 1996) as a physical model. We may apply the concept of the ferrovesicle to a magnetite cluster if we assume that (1) the magnetites in the cluster in situ are dispersed in a liquid, thereby constituting a magnetic fluid, and (2) a cluster is enclosed by a biological membrane.
3. The mathematical model of the ferrovesicle, first given by Bacri et al. (1996), is developped further. Now the equilibrium shape of the ferrovesicle can be derived by using a more general formula based on the concept of total energy. The expanded model allows us to consider the effect of thermal energy fluctuations on vesicle shape and orientation.
4. It is shown that a ferrovesicle is deformed in the Earth's magnetic field $\boldsymbol{H}_0$ such that the long axis of the deformed ellipsoid is aligned with $\boldsymbol{H}_0$ (on time average). Since the orientation of the ferrovesicle indicates only the axial direction of $\boldsymbol{H}_0$ but not its polarity, a ferrovesicle also has the potential to serve as the basis of the so-called inclination compass of migratory birds.
5. It is demonstrated that osmotic pressure plays an important role in a possible magnetoreception mechanism based on a ferrovesicle. The active regulation of osmotic pressure makes it possible to measure magnetic field changes indirectly by counterbalancing magnetically induced shape changes. On the other hand, by increasing the osmotic pressure outside the ferrovesicle above a certain threshold value, the organism could determine the axial direction of $\boldsymbol{H}_0$ more precisely.
6. A further way to enhance the sensitivity of a single ferrovesicle is presented and quantitatively described. The ferrovesicle now is assumed to contain a magnetically stable single-domain particle (of size 50 nm or so) in its centre. Such a particle behaves like a compass needle, i.e. will be aligned with $\boldsymbol{H}_0$. Since the magnetic field of the inner particle is amplified by the magnetic fluid "shell" surrounding the particle, the magnetic pressure acting on the ferrovesicle membrane is also increased, thereby yielding larger deformations. It is shown that such a system is mechanically stable, i.e. the single-domain magnet is not driven out of the centre of the ferrovesicle.

Appendix A: Curvature elastic energy of a prolate vesicle

According to Helfrich (1973), the total bending energy of a vesicle membrane S can be written as

$$W_b = \int_S \left\{ K_c/2\,(c_1 + c_2 - c_0)^2 + K_G\, c_1\, c_2 \right\} dA \qquad (A1)$$

where c_1, c_2 are the two principal curvatures of the membrane, c_0 is its spontaneous curvature, K_c the bending rigidity, K_G the gaussian curvature modulus, and dA the area element on S. The integral over the second term in Eq. (A1), the gaussian curvature, is constant for deformations which do not change the topology of a surface and therefore is omitted in the following. By analogy to Zhong-can and

Helfrich (1989), we introduce the following quantities from differential geometry:

$$\begin{aligned} &\boldsymbol{Y}_i = \partial_i \boldsymbol{Y}, \quad \boldsymbol{Y}_{ij} = \partial_i \partial_j \boldsymbol{Y}, \quad g_{ij} = \boldsymbol{Y}_i \cdot \boldsymbol{Y}_j \\ &L_{ij} = \boldsymbol{Y}_{ij} \cdot \boldsymbol{n}, \quad g = \det(g_{ij}), \quad g^{ij} = (g_{ij})^{-1} \\ &\boldsymbol{n} = (\boldsymbol{Y}_i \times \boldsymbol{Y}_j)/\sqrt{g}, \quad \mathcal{H} = -(c_1 + c_2)/2 = 1/2\, g^{ij} L_{ij} \end{aligned} \tag{A2}$$

with $(i, j) = 1, 2$ and $\partial_1 = \partial/\partial\theta$, $\partial_2 = \partial/\partial\phi$. The g_{ij} are the components of the covariant metric tensor, $\boldsymbol{n}$ denotes the outward unit normal vector and $\mathcal{H}$ the mean curvature. The surface of an ellipsoid of revolution (axial ratio $k = b/a$) can be described by the vector

$$\boldsymbol{Y}(\theta, \phi) = a\,(k \sin\theta \cos\phi,\, k \sin\theta \sin\phi,\, \cos\theta) \tag{A3}$$

with $0 \le \theta \le \pi$ and $0 \le \phi \le 2\pi$. Inserting Eq. (A3) into Eq. (A2) yields

$$\begin{aligned} &g_{11} = a^2 \lambda^2, \quad g_{12} = g_{21} = 0, \quad g_{22} = a^2 k^2 \sin^2\theta \\ &L_{11} = -a k/\lambda, \quad L_{12} = L_{21} = 0, \quad L_{22} = -a k \sin^2\theta/\lambda \end{aligned}$$

with $\lambda^2 = (1 \pm \varepsilon_\pm^2 \cos^2\theta)$, where the minus sign applies to the prolate ellipsoid ($k \le 1$) with $\varepsilon_-^2 = 1 - k^2$, and the plus sign correspondingly to the oblate shape ($k \ge 1$) with $\varepsilon_+^2 = k^2 - 1$. Making use of rotational symmetry, the bending energy of Eq. (A1) becomes

$$W_\mathrm{b} = \pi K_\mathrm{c} \int_0^\pi \left(\frac{2 \pm \varepsilon_\pm^2 (1 + \cos^2\theta)}{a k (1 \pm \varepsilon_\pm^2 \cos^2\theta)^{3/2}} - c_0 \right)^2 \sqrt{g}\, \mathrm{d}\theta \tag{A4}$$

After substitution of $\cos\theta$ and subsequent integration, we arrive for the prolate ellipsoid[3] at

$$\begin{aligned} W_{\mathrm{b},-} = \pi K_\mathrm{c} \Bigg(&14/3 - 4 a c_0 + (4/3 + a^2 c_0^2) k^2 \\ &+ \frac{(2 + a^2 c_0^2 k^2)\, \arcsin(\varepsilon_-)}{\varepsilon_- k} - \frac{4 a c_0 k^2\, \mathrm{atanh}(\varepsilon_-)}{\varepsilon_-} \Bigg) \end{aligned} \tag{A5}$$

For small deformations of the sphere ($\varepsilon \ll 1$), we can approximate Eq. (A5) by

$$W_{\mathrm{b},-} \simeq 2\pi K_\mathrm{c} \left\{ (2 - c_0 R_0)^2 + \frac{4}{45} (6 - c_0 R_0) \varepsilon_-^4 + O(\varepsilon^6) \right\} \tag{A6}$$

where the constraint of constant surface area was included.

Appendix B: Magnetization of a ferrofluid in a spherical shell around a spherical SD particle

The static magnetic field H can be represented as the gradient of a potential Φ

$$H = -\nabla \Phi \tag{A7}$$

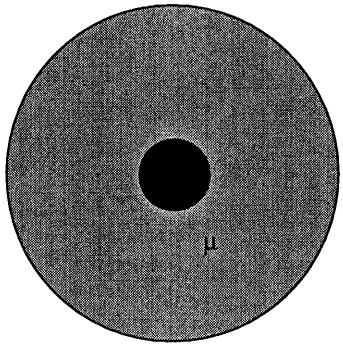

Fig. 8 A permanent magnet embedded in a spherical ferrofluid droplet

and is related to magnetic flux density B by

$$B = \mu H = (1 + 4\pi\chi) H = H + 4\pi M \tag{A8}$$

where μ and χ are magnetic permeability and susceptibility, respectively, and M denotes the macroscopic magnetization vector. Putting $\mathrm{div} B = 0$ in Eq. (A7) leads to

$$\Delta \Phi = 4\pi\, \mathrm{div} M \tag{A9}$$

if μ is constant[4]. The magnetic field distribution of equilibrium can thus be determined by means of potential theory.

Consider now an SD particle (magnetization M_S), spherical in shape (radius r_i), placed in the center of a spherical shell (radius R_0) filled with a ferrofluid of permeability μ (Fig. 8). The appropriate coordinates of this problem are spherical polar coordinates (r, θ, ϕ). The $\theta = 0$ axis is chosen as parallel to the magnetization of the inner SD particle. With this, the solution of Eq. (A9) for the three different regions is given by

$$r \le r_\mathrm{i} : \Phi_2 = -H_2\, r \cos\theta \tag{A10}$$

$$r_\mathrm{i} < r \le R_0 : \Phi_1 = \left(\frac{\gamma}{r^2} - H_1 r \right) \cos\theta \tag{A11}$$

$$r > R_0 : \Phi_0 = \left(\frac{\alpha}{r^2} - H_0 r \right) \cos\theta \tag{A12}$$

where the coefficients α, γ, H_1, and H_2 are to be determined by the boundary conditions; H_0 is the externally applied field, so that for $r \gg R_0$, we have $H = H_0$.

Across any boundary, the potential and the normal component of B are continuous, which leads to

$$\begin{aligned} \Phi_2(r_\mathrm{i}) &= \Phi_1(r_\mathrm{i}) \\ \Phi_1(R_0) &= \Phi_0(R_0) \\ -\mu \left(\frac{\partial \Phi_1}{\partial r} \right)_{r=r_\mathrm{i}} &= -\left(\frac{\partial \Phi_2}{\partial r} \right)_{r=r_\mathrm{i}} + 4\pi\sigma \\ -\mu \left(\frac{\partial \Phi_1}{\partial r} \right)_{r=R_0} &= -\left(\frac{\partial \Phi_0}{\partial r} \right)_{r=R_0} + 4\pi\sigma \end{aligned}$$

[3] The corresponding expression for the oblate shape, $W_{\mathrm{b},+}$, is obtained from $W_{\mathrm{b},-}$ by replacing $\arcsin(\varepsilon_-)/\varepsilon_-$ through $\mathrm{asinh}(\varepsilon_+)/\varepsilon_+$ and $\mathrm{atanh}(\varepsilon_-)/\varepsilon_-$ through $\arctan(\varepsilon_+)/\varepsilon_+$

[4] Strictly speaking, one cannot assume that the magnetic permeability of the ferrofluid is constant in the presence of a strong field gradient like that due to the inner permanent magnet

with $4\pi\sigma = M_n = \vec{M}\cdot\vec{n} = M_S\cos\theta$ being the magnetic surface charge, which leads to a jump in the normal magnetic field component across the surface of the SD particle.

With $q = R_0/r_i$, we obtain the coefficients as

$$\alpha = R_0^3\left(12\mu\pi M_S + H_0(q^3-1)(2\mu^2-\mu-1)\right)D^{-1}$$
$$H_1 = \left(3H_0(2\mu+1)q^3 - 8(\mu-1)\pi M_S\right)D^{-1}$$
$$\gamma = -R_0^3\left(3H_0(\mu-1) - 4(\mu+2)\pi M_S\right)D^{-1}$$
$$H_2 = \left(9H_0\mu q^3 - 4\pi M_S\left(2(q^3-1)+\mu(q^3+2)\right)\right)D^{-1}$$

where

$$D = q^3(2\mu+1)(\mu+2) - 2(\mu-1)^2$$

At the surface of the ferrofluid droplet, the magnetization is given as

$$M_{1,R_0} = \chi\,\frac{24\pi M_S + 3H_0(2+q^3+2\mu(q^3-1))}{q^3(2\mu+1)(\mu+2)-2(\mu-1)^2}\cos\theta \quad \text{(A13)}$$

For large values of q, the influence of the inner permanent magnetet reduces more and more, and we obtain the expression for the magnetization of a pure ferrofluid

$$M_F = \frac{3(\mu-1)H_0}{4\pi(\mu+2)} \quad \text{(A14)}$$

Appendix C: Levitation of an SD particle in the ferrovesicle

A general formula for the force acting on a body is

$$\boldsymbol{F} = \oint_S \boldsymbol{n}\,\boldsymbol{T}\,\mathrm{d}S \quad \text{(A15)}$$

(e.g. Landau and Lifshitz 1984), where the integration is performed over its surface S, $\boldsymbol{n}$ is the outward unit vector normal to the surface and $\boldsymbol{T}$ is a stress tensor.

According to the third Newtonian law, calculations of the force acting on a magnet by a surrounding magnetic medium may be replaced by calculating the force of the magnet exerted on the medium taken with negative sign (Rosensweig 1985; Berkovsky et al. 1993). For an isotropic homogeneous ferrofluid with an induced magnetization $\boldsymbol{M}$, Eq. (A15) can be rewritten as

$$\boldsymbol{F} = -(4\pi)^{-1}\oint_S\left[(\boldsymbol{M}\cdot\boldsymbol{n})^2/2 + \int_0^H M\,\mathrm{d}H'\right]\boldsymbol{n}\,\mathrm{d}S \quad \text{(A16)}$$

where the integration has to be performed over the interface S between magnet and ferrofluid. For a linear magnetic response, we have $\int_0^M M\,\mathrm{d}H' = (\mu-1)H^2/2$. The decomposition of $\boldsymbol{H}$ into its normal H_n and tangential H_t components together with Eq. (A16) leads to

$$\boldsymbol{F} = -(8\pi)^{-1}\oint_S\left[(\mu-1)^2H_n^2 + (\mu-1)H_t^2\right]\boldsymbol{n}\,\mathrm{d}S \quad \text{(A17)}$$

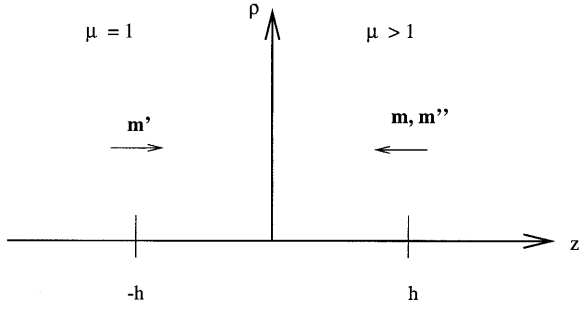

Fig. 9 Sketch of the method of mirrored charges

If $r_i \ll h \ll R_0$ then, in a first approximation, one may consider a magnet as a point dipole immersed in a ferrofluid occupying a half-space. For the sake of simplicity, we consider the case that the dipole moment $\boldsymbol{m}$ is directed to the surface. An advantage of such a model is that the rigorous solution can be found using the method of images (e.g. Landau and Lifshitz 1984). Let a dipole be placed at a distance $z = h$ from the plane $z = 0$, which separates the ferrofluid of permeability $\mu_2 = \mu$ from a non-magnetic substance with $\mu_2 = 1$ (Fig. 9). If $\boldsymbol{m}$ is normal to the surface, the dipole field in the infinite media is determined by the potential $\varphi_{dip} = \boldsymbol{m}\cdot\boldsymbol{r}/(\mu r^3)$, where $\boldsymbol{r}$ is radius-vector of the dipole. For the half-space one may seek the potential as the sum of the potentials of two point dipoles, $\boldsymbol{m}$ and a ficitious one $\boldsymbol{m}'$ directed antiparallel to $\boldsymbol{m}$ and disposed symmetrically to the plane outside the fluid (Fig. 9):

$$\varphi_1 = \frac{m(z+h)}{\mu r^3} - \frac{m'(z-h)}{\mu r'^3} \quad \text{(A18)}$$

where $r = \sqrt{(z+h)^2+\rho^2}$, $r' = \sqrt{(z-h)^2+\rho^2}$ are the distances from $\boldsymbol{m}$ and $\boldsymbol{m}'$, respectively, and z, ρ are cylindrical coordinates. The field in the non-magnetic media may be expressed as

$$\varphi_2 = \frac{m''(z+h)}{r^3} \quad \text{(A19)}$$

Here $\boldsymbol{m}''$ is another ficitious dipole displaced in the same location as $\boldsymbol{m}$. The validity of this solution can be readily checked by applying the boundary conditions to the plane $z = 0$, i.e.

$$\varphi_1 = \varphi_2 \quad \text{and} \quad \mu_1\frac{\partial\varphi_1}{\partial z} = \frac{\partial\varphi_2}{\partial z}$$

which leads to $m' = m(\mu-1)/(\mu+1)$.

For the magnetic field $\boldsymbol{H} = (H_n, H_t)$ we have

$$H_n = -\frac{\partial\varphi_1}{\partial z}\Big|_{z=0} = \frac{2m}{\mu(\mu+1)}\,\frac{2h^2-\rho^2}{(h^2+\rho^2)^{(5/2)}} \quad \text{(A20)}$$

$$H_t = -\frac{\partial\varphi_1}{\partial\rho}\Big|_{z=0} = \frac{2m}{(\mu+1)}\,\frac{3h\rho}{(h^2+\rho^2)^{(5/2)}} \quad \text{(A21)}$$

Owing to the symmetry of the potential φ_1, the only non-zero force component acting on the body is $-F_z$. Making use of the equality

$$\int_0^\infty \left(\frac{2h^2-\rho^2}{r^5}\right)^2 \mathrm{d}\rho = \int_0^\infty \left(\frac{3h\rho}{r^5}\right)^2 \rho\,\mathrm{d}\rho = \frac{3}{8h^4} \qquad \text{(A22)}$$

together with Eqs. (A17), (A20) and (A21) we obtain the force acting on $\boldsymbol{m}$ (the "image force") as

$$F(h) = \frac{6m^2}{(2h)^4}\,\frac{\mu-1}{\mu(\mu+1)} \qquad \text{(A23)}$$

Obviously, this is just the repulsion force between the two dipoles, $\boldsymbol{m}$ and $\boldsymbol{m}'$, separated by their mutual distance $2h$. This expression can be directly obtained from the usual formula $\boldsymbol{F}=(\boldsymbol{m}\nabla)\boldsymbol{H}$, which due to Eq. (A18) is equivalent to Eq. (A23). The corresponding potential is

$$U(h) = -\int_{-\infty}^{-h} F(h')\,\mathrm{d}h' = \frac{m^2}{(2h)^3}\,\frac{\mu-1}{\mu(\mu+1)} \qquad \text{(A24)}$$

In the same manner it can be shown that for the case where $\boldsymbol{m}$ is parallel to the plane, the corresponding forces are as much as twice lower than for $\boldsymbol{m}$ perpendicular to the surface, which means that the latter orientation is more preferred in zero external field. The solution for a dipole situated within a sphere cannot be found analytically. Therefore, this task must be treated either by approximated methods or numerically. The simplest approximation may be done using the approach suggested by Bastovoj et al. (1988), which is valid for the case of relatively low susceptibility χ. One may put $H=H_0$ where H_0 is the magnetic field from a magnet in vacuum such that $M=\chi H_0$; then, leaving only the term of first order in χ in Eq. (A16), we get

$$\boldsymbol{F} = -(8\pi)^{-1}\oint_S (\mu-1)H^2\,\boldsymbol{n}\,\mathrm{d}S \qquad \text{(A25)}$$

which can be readily solved. For the case stated above we have

$$F(h) = \frac{3(\mu-1)m^2}{(2h)^4} \qquad \text{(A26)}$$

where Eq. (A22) was accounted for. In the limit of low χ, Eq. (A26) approaches Eq. (A23). Now we consider the more realistic situation where a small spherical SD particle is immersed in a spherical ferrofluid droplet. The force $\boldsymbol{F}_{\mathrm{SD}}(r_\mathrm{d})$, were r_d is its displacement from the centre, and the corresponding potential U_{SD} were numerically calculated using the approximative formula of Eq. (A17) for the case that the grain's moment $\boldsymbol{m}$ is directed along the displacement. The function U_{SD}/kT is shown for $R_0=10\,r_\mathrm{i}$, and $r_\mathrm{i}=50$ nm in Fig. 10 for $\chi=0.1$ and $\chi=1$. It can be seen that for the case of low χ, the agreement between the two different curves is really good, whereas for a more concentrated ferrofluid with $\mu=2$ the difference is substantial. For our purpose, however, it is enough to demonstrate that in both cases a particle of size $r_\mathrm{i}=50$ nm avoids to be too close to the surface of the ferrofluid droplet. This can be shown with the Boltzmann distribution giving the probability for a grain to stay at a distance h from the surface as proportional to

$$\exp\left(-\frac{U_{\mathrm{dip}}}{kT}\right) = \exp\left(-\frac{\pi M_\mathrm{S}^2 v}{6kT}\left(\frac{r_\mathrm{i}}{h}\right)^3\frac{\mu-1}{\mu(\mu+1)}\right) \qquad \text{(A27)}$$

with $m=vM_\mathrm{S}$ and $v=(4\pi/3)r_\mathrm{i}^3$. Hence, the particle is bound to the centre of the droplet inside region $r_\mathrm{d}<(3-6)\,r_\mathrm{i}$ depending on particular value of μ.

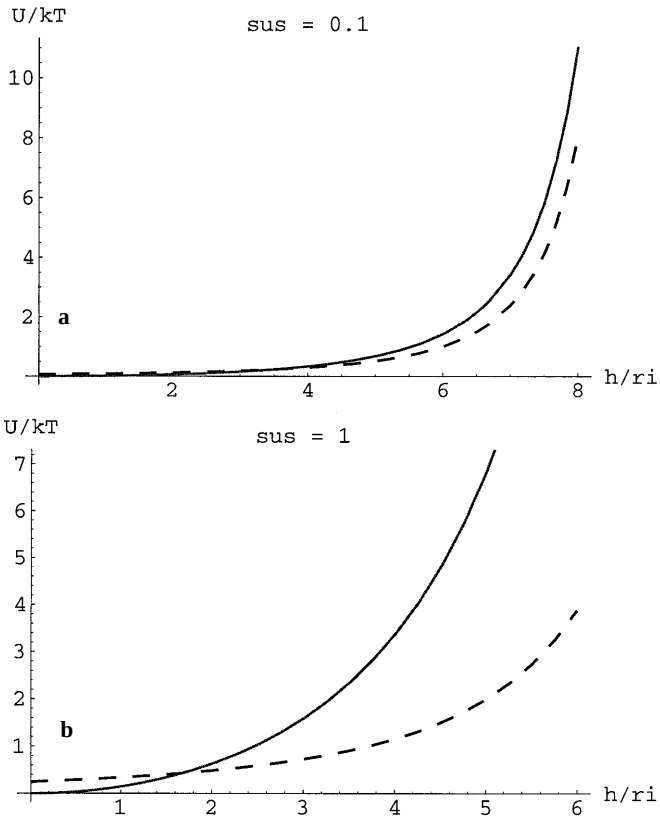

Fig. 10 a, b Potential energy of an SD particle (radius $r_\mathrm{i}=50$ nm) in a ferrofluid drop (radius $R_0=10\,r_\mathrm{i}$) as a function of its displacement h/r_i from the centre of the drop. **a** $\mu=1.1$; **b** $\mu=2$. *Solid lines* demonstrate U/kT as calculated from the exact solution for a point dipole situated in the ferrofluid in a planar halfspace; *dashed lines* show U/kT for the approximation of a spherical SD grain placed in spherical droplet. It can be seen that the SD particle indeed avoids to be too close to the surface in region $h<6\,r_\mathrm{i}$

Acknowledgements We are very grateful to M. Hanzlik, K. Fabian and N. Petersen for valuable suggestions and carefully reading the manuscript. We would like to thank E. Holtkamp-Rötzler and G. Fleissner for stimulating discussions. This investigation was supported by a grant from the Volkswagen Stiftung, by grant Pe 173/9-3 from the Deutsche Forschungsgemeinschaft (DFG) and by a travel award to V. S. from the Deutscher Akademischer Austauschdienst (DAAD).

References

Bacri JC, Salin D (1982) Instability of ferrofluid droplets under magnetic field. J Phys Lett 43: L 649–654

Bacri JC, Salin D, Massart R (1982) Study of the deformation of ferrofluid droplets in a magnetic field. J Phys Lett 43: L 179–184

Bacri JC, Cabuil V, Cebers A, Menager C, Perzynski R (1996) Flattening of ferro-vesicle undulations under a magnetic field. Europhys Lett 33: 235–240

Bastovoj VG, Berkovsky BM, Vislovitch AN (1998) Introduction to thermomechanics of magnetic fluids. Hemisphere, Washington

Bean CP (1955) Hysteresis loops of mixtures of ferromagnetic micropowders. J Appl Phys 26: 1381–1383

Berkowsky BM, Medvedev VF, Krakov MS (1993) Magnetic fluids. Oxford University Press, Oxford

Blakemore RP (1975) Magnetotactic bacteria. Science 19: 377–379

Blums E, Cebers A, Maiorov MM (1988) Magnetic fluids. de Gruyter, Berlin

Edmonds DT (1992) A magnetite null detector as the migrating bird's compass. Proc R Soc (Lond) Ser B 249: 27–31

Elmore WC (1938) Magnetization of colloids. Phys Rev 54: 1092–1095

Evans EA, Rawicz W (1990) Entropy-driven tension and bending elasticity in condensed-fluid membranes. Phys Rev Lett 64: 2094–2097

Fabian K, Kirchner A, Williams W, Heider F, Leibl T, Hubert A (1996) Three-dimensional micromagnetic calculations for magnetite using fit. Geophys J Int 124: 89–104

Frankel RB, Blakemore RP (1980) Navigational compass in magnetic bacteria. J Magn Magn Mater 15–18: 1562–1564

Gould JL, Kirschvink JL, Deffeyes KS (1978) Bees have magnetic remanence. Science 201: 1026–1028

Helfrich W (1973) Elastic properties of lipid bilayers: theory and possible experiments. Z Naturforsch 28c: 693–703

Holtkamp-Rötzler E, Fleissner G, Hanzlik M, Petersen N (1997) The morphological structure of a possible magnetite-based magnetoreceptor in birds. Ann Geophys 15 [Suppl. I C]: 117

Kirschvink JL (1992a) Comment on "constraints on biological effects of weak extremely-low-frequency electromagnetic fields". Phys Rev A 46: 2178–2186

Kirschvink JL (1992b) Discrimination of low-frequency magnetic fields by honeybees: biophysics and experimental tests. In: Corey DP, Roper SD (eds) Sensory transduction. (Society of General Physiologists series, vol 47) Rockefeller University Press, New York, pp 225–240

Kirschvink JL, Gould JL (1981) Biogenic magnetite as a basis for magnetic field detection in animals. BioSystems 13: 181–201

Kirschvink JL, Diaz-Ricci JC, Nesson MH, Kirschvink SJ (1993) Magnetite-based magnetoreceptors in animals: structural, behavioral, and biophysical studies. Technical Report TR-102008, Electric Power Research Institute, Palo Alto, Calif

Kwok R, Evans EA (1981) Thermoelasticity of large lecithin bilayer vesicles. Biophys J 35: 637–652

Landau LD, Lifshitz EM (1984) Electrodynamics of continuous media. (Course of theoretical physics, vol 8) Pergamon Press, Oxford

Lowenstam HA (1962) Magnetite in denticle capping in recent chitons (polyplacophora). Geol Soc Am Bull 73: 435–438

Mann S, Sparks NH, Walker MM, Kirschvink JL (1988) Ultrastructure, morphology and organization of biogenic magnetite from sockeye salmon, *Oncorhynchus nerka*: implications for magnetoreception. J Exp Biol 140: 35–49

Néel L (1949) Théorie du trainage magnétique des ferromagnétiques en grains fins avec applications aux terres cuites. Ann Géophys 5: 99–136

Presti D, Pettigrew JD (1980) Ferromagnetic coupling to muscle receptors as a basis for geomagnetic field sensitivity in animals. Nature 285: 99–101

Quinn TP, Brannon EL (1982) The use of celestial and magnetic cues by orienting sockeye salmon smolts. J Comp Physiol 147: 547–552

Rosensweig RE (1985) Ferrohydrodynamics. Cambridge University Press, Cambridge

Sackmann E (1994) Membrane bending energy concept of vesicle- and cell-shapes and shape-transitions. FEBS Lett 346: 3–16

Sakaki Y, Motomiya T (1990) Possible mechanism of biomagnetic sense organ extracted from sockeye salmon. IEEE Trans Magn 26: 1554–1556

Semm P, Beason RC (1990) Responses to small magnetic variations by the trigeminal system of the bobolink. Brain Res Bull 25: 735–740

Semm P, Demaine C (1986) Neurophysiological properties of magnetic cells in the pigeons's visual system. J Comp Physiol A 159: 619–625

Semm P, Nohr D, Demaine C, Wiltschko W (1984) Neural basis of the magnetic compass: interactions of visual, magnetic and vestibular inputs in the pigeon's brain. J Comp Physiol A 155: 283–288

Torres de Araujo FF, Pires MA, Frankel RB, Bicudo CEM (1986) Magnetite and magnetotaxis in algae. Biophys J 50: 375–378

Walcott C, Gould JL, Kirschvink JL (1979) Pigeons have magnets. Science 205: 1027–1029

Walker MM, Kirschvink JL, Chang S-BR, Dizon AE (1984) A candidate magnetic sense organ in the yellowfin tuna, *Thunnus albacares*. Science 224: 751–753

Walker MM, Quinn TP, Kirschvink JL, Groot C (1988) Production of single-domain magnetite throughout life by sockeye salmon, *Oncorhynchus nerka*. J Exp Biol 140: 51–63

Walker MM, Diebel CE, Haugh CV, Pankhurst PM, Montgomery JC (1997) Structure and function of the vertebrate magnetic sense. Nature 390: 371–376

Wiltschko R, Wiltschko W (1995) Magnetic orientation in animals. (Zoophysiology, vol 33) Springer, Berlin Heidelberg New York

Wiltschko W, Wiltschko R (1972) Magnetic compass of european robins. Science 205: 1027–1029

Winklhofer M (1998) Theoretische Modelle der Magnetfeldrezeption auf der Grundlage biologischer Magnetit-Teilchen. Dissertation, Ludwig-Maximilians-Universität, München

Yorke ED (1979) A possible magnetic transducer in birds. J Theor Biol 77: 101–105

Zhong-can O-Y, Helfrich W (1989) Bending energy of vesicle membranes: general expressions for the first, second, and third variation of the shape energy and applications to spheres and cylinders. Phys Rev A 39: 5280–5288